Experimental investigation of adaptive impedance matching for a MIMO terminal with CMOS SOI tuners

Vasilev, Ivaylo; Lindstrand, Jonas; Plicanic, Vanja; Sjöland, Henrik; Lau, Buon Kiong

Published in:
IEEE Transactions on Microwave Theory and Techniques

DOI:
10.1109/TMTT.2016.2546244

2016

Document Version:
Peer reviewed version (aka post-print)

Experimental Investigation of Adaptive Impedance Matching for a MIMO Terminal with CMOS-SOI Tuners

Ivaylo Vasilev, *Student Member, IEEE*, Jonas Lindstrand, *Student Member, IEEE*, Vanja Plicanic, *Member, IEEE*, Henrik Sjöland, *Senior Member, IEEE* and Buon Kiong Lau, *Senior Member, IEEE*

***Abstract*—It is well known that user proximity introduces absorption and impedance mismatch losses that severely degrade multiple-input multiple-output (MIMO) performance of handset antennas. In this work, we experimentally verified the potential of adaptive impedance matching (AIM) to mitigate user interaction effects and identified the main AIM gain mechanism in realistic systems. A practical setup including custom-designed CMOS silicon-on-insulator (SOI) impedance tuners implemented on a MIMO handset was measured in three propagation environments and 10 real user scenarios. The results indicate that AIM can improve MIMO capacity by up to 42% equivalent to 3.5 dB of multiplexing efficiency (ME) gain. Taking into account the measured losses of 1 dB in the integrated tuners, the maximum net ME gain is 2.5 dB suggesting applicability in practical systems. Variations in ME gains of up to 1.5 dB for different hand-grip styles were mainly due to differences in impedance mismatch and tuner loss distribution. The study also confirmed earlier results on the significant differences in mismatch and absorption between phantoms and real users, in which the phantoms underestimated user effects and therefore AIM gains. Finally, propagation environments of different angular spreads were found to give only minor ME gain variations.**

***Index Terms* - CMOS ICs, impedance matching, antennas and propagation, MIMO and cellular systems.**

I. Introduction

THE cellular telecommunications industry association (CTIA) has specified that handset antennas are required to operate efficiently in free space as well as in close proximity to users while browsing, texting and calling [1]. Nevertheless, designing an efficient RF front end in the confined space of personal communication devices, with high robustness to user interaction is a challenging task [2]. Closely spaced antenna elements exhibit high mutual coupling and excite highly correlated radiation patterns that severely degrade the achievable capacity [2]. In addition, the proximity of users can lead to severe absorption and mismatch losses that further reduce antenna efficiency and therefore MIMO capacity [2].

In recent years, adaptive impedance matching (AIM) has been proposed for optimizing MIMO performance by improving total efficiency and correlation [3]-[9]. The key difference in using AIM for user effect compensation between single- and MIMO antennas in compact terminals is that single-antenna AIM only mitigates impedance mismatch (e.g. [10]), whereas MIMO antenna AIM can also influence the coupling and antenna pattern, and hence correlation. As summarized in Table I, the first studies on AIM for MIMO antennas were fundamental in nature and based on simulations with no user and ideal half-wave dipole antennas [3]-[5]. The initial work showed that significant MIMO performance gains could be achieved using AIM by improving total efficiency and correlation, as well as obtaining a trade-off between them for optimal capacity performance.

TABLE I
COMPARISON OF AIM STUDIES FOR MIMO ANTENNAS

Ref.	Tuner	Antenna	User	Channel
[3]-[5]	sim.	sim. dipoles	none	sim. APS
[6]	sim.	sim. handset antennas	sim.	sim. uniform 3D APS only
[7]	sim.	meas. handset antennas	meas. phantom	sim. APS
[8]	sim.	meas. handset antennas	meas. phantom	meas. indoor
[9]	meas. (large)	meas. handset antennas	meas. phantom	meas. indoor and outdoor
This paper	meas. (compact)	meas. handset antennas	meas. phantom vs. real	meas. indoor

NB. sim.= simulated; meas.= measured; APS = angular power spectrum

To investigate the practicality and the underlying mechanisms of AIM for MIMO terminal application, subsequent studies shown in Table I progressively adopted more realistic conditions of terminal antennas, tuner, user and propagation channel [6]-[9]. Besides validating the promising AIM gains from simulation studies, these studies facilitated useful insights on performance gains from AIM. In particular, highly coupled and narrowband MIMO antennas can benefit from large AIM gains since user proximity (i.e., represented by a phantom user) tends to reduce coupling and cause severe detuning, the latter of which can be effectively compensated through retuning [6]-[8]. The Maury mechanical tuners used in [9] demonstrated that the retuning of mismatched terminal antennas should take into account the increasing insertion loss

Manuscript received April 16, 2015; revised November 13, 2015. This work was supported in part by VINNOVA under grant no. 2009-04047, and in part by Vetenskapsrådet under grant no. 2010-468.

I. Vasilev, J. Lindstrand, H. Sjöland and B. K. Lau are with the Department of Electrical and Information Technology, Lund University, 221 00 Lund, Sweden (e-mail: {Ivaylo.Vasilev, Jonas.Lindstrand, Henrik.Sjöland, Buon_ Kiong.Lau}@eit.lth.se). H. Sjöland is also with Ericsson Research, Ericsson AB, 22183 Lund, Sweden.

V. Plicanic is with the Network Technology Laboratory, Sony Mobile Communications AB, 221 88 Lund, Sweden (email: Vanja.Plicanic Samuelsson@sonymobile.com).

of the tuner away from the 50 Ω state. Furthermore, the directional characteristics of the channel with respect to the multi-antenna patterns are shown to have a significant influence on the performance gain from AIM [8], [9]. Gains of up to 2.1 dB and 1.6 dB were measured in an indoor and outdoor propagation scenario, respectively [9]. Nevertheless, despite the promising results in [3]-[9], neither compact integrated tuners nor real users have yet been considered. For the single-antenna case, integrated tuners have been designed for many years, such as the 0.35-μm adaptive CMOS circuit based on several switched shunt capacitors and external inductors proposed for the 2.4 GHz ISM band [10]. However, it was not until recently that tuning circuits with significantly better performance were developed and aimed for commercial AIM implementation. For example, the RF-MEMS tuning module reported in [11] features 0.3 dB insertion loss at 850 MHz. In [12], an integrated matching network for high band operation (2.5-2.69 GHz) was designed in a 130 nm CMOS-silicon-on-insulator (CMOS-SOI) process. For antenna impedances with a voltage standing wave ratio (VSWR) of 5, the tuner was able to significantly reduce mismatch losses. However, there is no real-world verification of these circuits in realistic environments and user scenarios. Recent studies also investigated other key aspects of adaptive RF front-ends such as antenna-power amplifier mismatch [13] real-time complex impedance measurement [14]. Yet, only limited verification in realistic conditions was done.

In [15], a study involving 60 users revealed that a closed-loop tuner system can provide AIM gains of up to 3.6 dB by mitigating antenna mismatch. Moreover, the mismatches encountered with real users were significantly more severe than those with phantom users complying with CTIA over-the-air test specifications. However, the study involved only a single-antenna terminal with no verification in realistic propagation conditions through channel measurements.

In the context of the previous work, this paper makes the following contributions (see also Table 1):

- RF design, evaluation and measurement of a complete AIM system based on a state-of-the-art tuner [16] custom-designed for a specific MIMO handset in a CMOS-SOI process applicable for mass production.
- First of its kind practical verification of an AIM system in realistic propagation conditions and user scenarios probing the applicability of AIM in real systems with existing low-cost technologies. The system achieved promising net power gains of 0.8-3 dB.
- Analysis of the capacity and multiplexing efficiency performance of the AIM-equipped MIMO handset in three environments with both realistic and phantom user scenarios reveals that the system performance gain mainly depends on the trade-off between the tuner loss and the achieved mismatch reduction. The weak influence of the channel on AIM gain is due to the inability of AIM to adapt the antenna patterns to the channel for improved performance.
- Analysis of the impact of five fundamentally different hand-grip styles on AIM performance shows that the grips provided different gains depending on the proximity of the palm or fingers to the radiating elements which led to different mismatch and absorption loss characteristics.
- Comparison of phantom hand-grips with real user hand-grips establishes that the phantom cases underestimated user-effects and therefore AIM gains, highlighting the importance of involving real users in the study of achievable AIM gains.

It should be noted that the approach taken in this paper is to minimize the tuner loss by limiting the tuner state coverage according to the expected impedance mismatch for the given MIMO handset antennas. As such, the AIM system could achieve a lower loss without sacrificing the coverage of optimal states. The reduced search space also facilitated the use of a relatively small number of states, which was also exploited to limit channel measurement time for exhaustive search. Consequently, this work focuses on potential RF signal improvements with AIM rather than algorithm development for finding optimal matching states; the latter being more critical for generic AIM systems targeting wide coverage and assume no prior knowledge of the antennas or user effects.

The paper is structured as follows. Section II presents the impedance tuner and the MIMO terminal prototype used. The measurement setups and figures of merits are detailed in Section III. Section IV provides the results and analysis and Section V concludes the paper.

II. AIM System and Antenna-Tuner Prototype

A. *Impedance Tuner System*

The AIM tuner chip featuring programmable capacitors and digital control was designed in-house and fabricated by STMicroelectronics using their 130 nm CMOS-SOI process [16]. It is noted that even though micro-electro-mechanical systems (MEMS) outperform CMOS in power handling and loss characteristics, the MEMS process is not as mature as CMOS. Hence, the MEMS process incurs high production cost, low volume capabilities and reliability issues [17]. Moreover, with the SOI process used in this work we can obtain improved RF performance over standard CMOS processes, especially in power handling and linearity [16]. The circuit schematic, printed circuit board (PCB) picture of the impedance tuner system, and capacitor bank circuit are shown in Figs. 1(a), 1(b) and 1(c), respectively. The system was designed as a double π-network and it comprised three programmable capacitors (C1, C2 and C3), two off-chip inductors (L1 = L2 = 7.4 nH), decoupling capacitors and RF chokes. The chip includes three identical 5-bit programmable capacitors with digital control [16] with a total chip area of 0.8 x 2 mm^2. The PCB area is 10 x 15 mm^2. Figure 1(c) shows the capacitor bank circuit where R = 275 kΩ is the gate resistor, C = 190 fF is the custom designed capacitor, VC indicates the control voltage and W1-W8 indicates the transistors used for the digital control [16].

The tuner system was characterized in detail in [16] over the frequency range 700-900 MHz. It offers state-of-the-art

performance: 1) a matching domain with coverage region of VSWR = 6.5, 2) in-band linearity with measured output third-order intercept point (OIP3) exceeding 55 dBm for all states, 3) power handling capabilities for both uplink and downlink, with the measured input power of the system being 33 dBm when limiting the spurious emissions to -30 dBm. In practice, the tuner system will be placed immediately adjacent to the antenna (see Fig. 1) in order to handle severe mismatches before they reach the more sensitive components in the front-end-module (FEM).

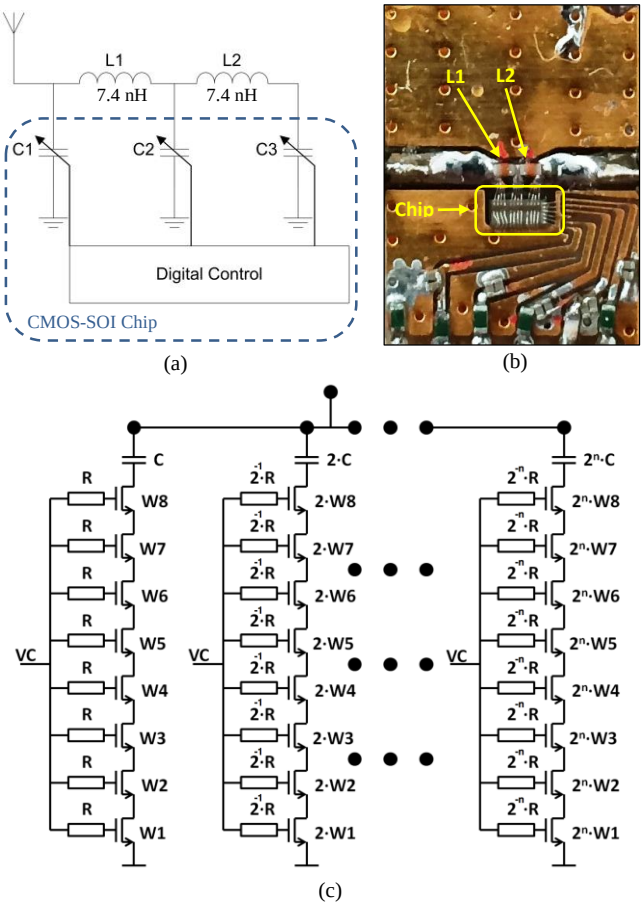

Fig. 1. (a) CMOS-SOI tuner circuit schematic; (b) PCB with chip and decoupling networks and (c) capacitor bank circuit (R = 275 kΩ; C = 190 fF; VC – control voltage and W1-W8 transistors).

Figure 2(a) shows the measured impedance state coverage of the tuner system. The programmable capacitor design was optimized for the tuning circuit to handle the measured impedances of an inverted-F antenna (IFA) based MIMO terminal prototype that was subjected to several representative one-hand and two-hand user interactions [7]-[9]. This consideration led to a greater emphasis on the capacitive states in the matching domain. Nevertheless, some variations in the convergence region are possible by changing inductors L1 and L2 shown in Fig. 1(a). Since each of the three on-chip programmable capacitors has a 5-bit resolution, the total number of available impedance states is $2^5 \times 2^5 \times 2^5 = 32768$ (i.e. the solid region in Fig. 2). A preliminary study of user effects in the MIMO handset used provided information of the expected input impedances, which served as design criteria for the impedance tuner and for selecting the tuner states to be verified. For example, the measured input impedance of the antenna in different user scenarios was used to define the region with a dense tuner state distribution. To limit the measurement time, only 22 states were used in this study, with more states chosen around the expected impedances of the given antenna-channel setup. The digital control (CLK and DATA signaling) of the tuner system was provided by an Atmel microcontroller [18], whereas results post-processing was done in LabView.

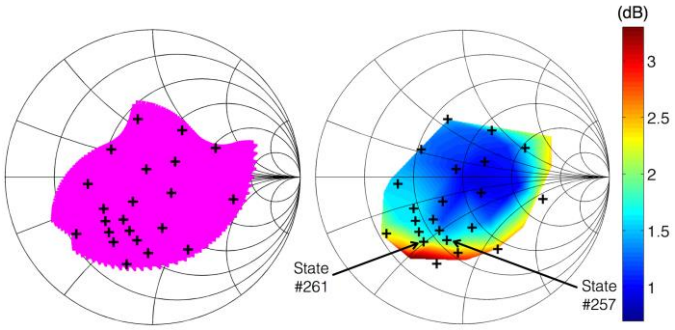

Fig. 2. CMOS-SOI tuner (a) measured coverage (solid region) and (b) measured loss (mismatch and resistive) with the impedance states used for the propagation measurements (+) at 845 MHz. State #257 and #261 are shown.

Detailed tuner loss measurements were performed for 39 impedance states at different VSWR and phase spreading through the coverage region of the tuner. The setup in [16] was used for the mismatch loss (ML) and resistive loss (RL) (or insertion loss) measurements. Figure 2(b) shows the color map of the combined tuner loss (ML+RL) obtained by interpolating the measurements from the 39 states. The 22 states used for this study are superimposed on the color map data. It can be seen that the loss increases for higher VSWRs (1 dB at VSWR = 1 and 3.5 dB at VSWR = 4.9). Therefore, applying the tuner on well matched antennas (input impedance of 50 Ω or VSWR = 1) will result in a net power loss of 1 dB. Consequently, impedance tuners are only beneficial in cases of significant user-induced mismatch (high VSWR), where the power gain from reducing mismatch exceeds the tuner loss [19]. In [7], AIM gains of up to 4.8 dB were measured in a two-hand grip. However, this number is optimistic as it considered neither tuner losses nor its variations with VSWR. From Fig. 2(b), a 2.5 dB increase in tuner losses can be observed for an increase in VSWR from 1 to 4.9. Hence, even though the AIM gains are high at high VSWR, the tuner losses also increase. Therefore, the optimal matching state for a given setup is a tradeoff between reducing mismatch and maintaining low tuner losses. In this context, one of the key contributions of this work is to experimentally establish the true potential of AIM under realistic operating environments, taking into account tuner losses.

B. MIMO Antenna-Tuner Prototype

Two MIMO terminal antenna prototypes were used in this study: Prototype A (i.e., Prototype A in [7]) and Prototype B. Prototype B, as shown in Figs. 3 and 4, is identical in design to Prototype A, except for the external PCBs added to accommodatethe integrated impedance tuner system (see Fig.

3) and a battery board (see Fig. 4) used for powering the chips during operation. Therefore, Prototype A (with no tuners) served as a reference prototype. Both prototypes consist of two identical IFAs placed in mirror symmetry along the two shorter edges of the ground plane. The IFAs cover LTE Band 18 (815-875 MHz) and LTE Band 9 (1.75-1.88 GHz). The total volume of each prototype is $130 \times 66 \times 9$ mm^3. In this work, only LTE Band 18 was considered, since the lower band is more challenging for multi-antenna implementation due to space constraint [2]. Moreover, at lower bands (below 1 GHz) both the antenna elements and the terminal chassis tend to radiate [2], which makes it more likely for the user to disturb the radiation. Therefore, user effects were found to be more severe at lower bands [19].

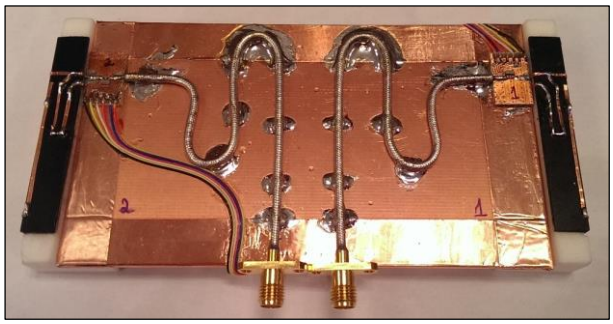

Fig. 3. Prototype B – prototype with integrated tuners (top view).

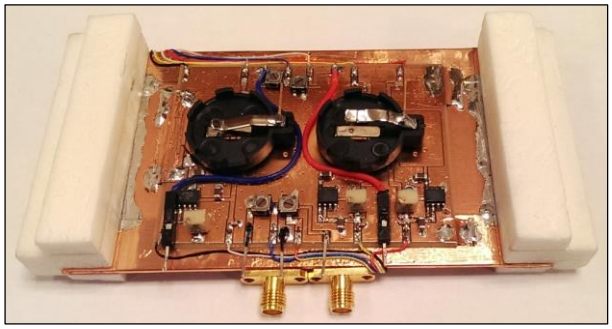

Fig. 4. Prototype B – prototype with integrated tuners (bottom view).

As described in [7], Prototype A offers measured total efficiencies and envelope correlation in free space (FS) of -3.9 dB/-3.4 dB (port 1/port 2) and 0.4, respectively, at 860 MHz. However, based on channel measurements performed during this study in a shielded room (with rich multipath), Prototype B that was equipped with the integrated tuners and the battery board was found to provide a substantially lower envelope correlation (of 0.2) than that of Prototype A (0.5) at the 50 Ω state. This correlation difference was due to structural changes in the terminal chassis (i.e., addition of external PCBs, components and wiring) contributing to decorrelation between the antenna ports [20], [21]. In addition, due to tuner losses, the total antenna efficiencies and mutual coupling of Prototype B at the 50 Ω state is expected to be 1 dB and 2 dB lower than Prototype A, respectively.

Figure 4 shows the battery board that provided regulated dc power to the tuner system, to avoid using a power cable that could disturb the measurement. It contained three voltage regulators, seven potentiometers and two battery holders fitting four 3V CR2025 batteries. The five pins (i.e. exposed wire tips) at the lower end of the board were used to connect the CLK and DATA signals for each of the tuners as well as a common GND signal to the Atmel microcontroller.

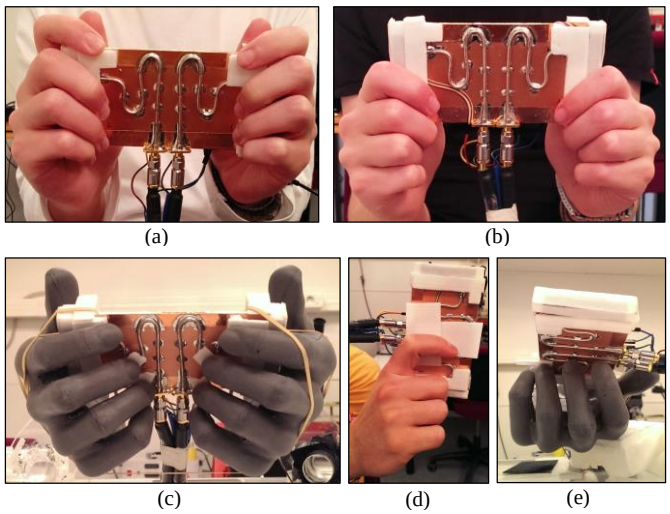

(a) (b) (c) (d) (e)

Fig. 5. User scenario setups: (a) firm grip (FI), (b) freestyle grip (FR), (c) two hands with IndexSAR phantoms (TH-P), (d) one hand (OH), and (e) one hand with IndexSAR phantom (OH-P).

III. Measurement Setup and Evaluation Method

A. User Scenarios

In this study, apart from the FS (no user) reference, five user scenarios were considered for Prototype B: two one-hand grips (OH and OH-P in Fig. 5) and three two-hand grips (FI, FR and TH-P in Fig. 5). Both real user test subjects and IndexSAR hand phantoms were used. The focus of this study was on the firm (FI) and freestyle (FR) two-hand grips (in landscape orientation), each involving 10 test subjects to obtain statistically relevant data. The number of test subjects was limited to 10 due to the relatively long measurement time. The 10 test subjects were between 26-39 years old and of average build, with three being females. The measurement time for the 2×2 MIMO channel transfer function of each setup (of user, handgrip and environment) took about 30 minutes. The bottleneck in the measurement time was the 10-snapshot averaging used by the four-port Agilent E5071C vector network analyzer (VNA) for each of the 22 tuner states, with the intermediate frequency bandwidth (IFBW) of the VNA set to 2 kHz. For the FI grip (see Fig. 5(a)), the 10 users were asked to cover as much of the terminal edges as possible with their two hands, without touching the ground plane or affecting the screen area. On the other hand, for the FR grip (see Fig. 5(b)), the users were asked to hold the terminal with both hands in a natural way. The two-hand grip with hand phantoms (TH-P) of Fig. 5(c) was reproduced from [9]. The one-hand scenarios with the phantom hand (OH-P) and real user hand (OH) shown in Fig. 5(d) and 5(e) were designed as two distinct cases where one of the two antennas was more affected by user interaction.

B. Measured Environments

Three different propagation environments were measured: shielded room (SR), line-of-sight (LOS) and non-line-of-sight (NLOS). The first environment SR was a shielded room used for verification of RF devices (see Fig. 6(a) and Fig. 7(a)). SR

was a rich multipath environment, due to the reflective walls and abundance of scattering objects. The transmit array (Tx) was kept fixed at the same position while the receive array (Rx) (i.e., Prototype A without user hands and Prototype B with user hands in a sitting posture) was measured over a rectangular grid of 9 positions at one wavelength (λ) spacing (at 800 MHz). Together with frequency realizations, the multiple measurements over the grid were used to average out small-scale fading. The transmit antenna array (see Fig. 6(a)) consisted of two wideband monopole antennas of one wavelength spacing at 800 MHz that are identical in design and fabrication to the ones used in [9]. The ground planes were positioned vertically on a tripod at a height of 1.8 m from the floor level. For the cases with user, the test subject (or IndexSAR phantom hands) was oriented to face the transmit array. The reference free-space cases were measured with Prototype A held up by the rigid feed cables, at about the same height and orientation as the corresponding user cases, with the top side facing the transmit array. To isolate the near-field influence of the hand(s) from the shadowing effect of the torso for the FR, FI and OH cases, these three reference cases were performed with a test subject in approximately the same sitting posture as the cases with user hand(s) but with hands(s) and arm(s) kept far away from the prototype. All five handgrips described in Section III-A were tested in this environment: two with phantoms (OH-P, TH-P), one (OH) with a single real user and two (FR, FI) with 10 test subjects.

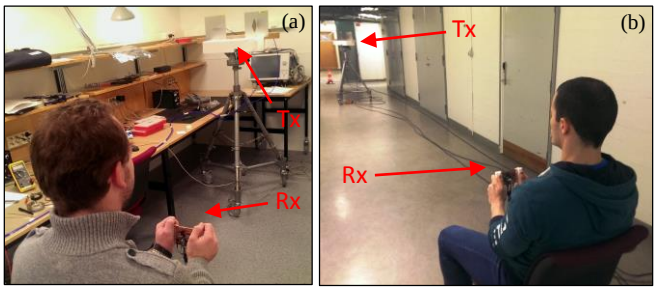

Fig. 6. Measurement setup: (a) shielded room environment and (b) basement corridor environment (LOS).

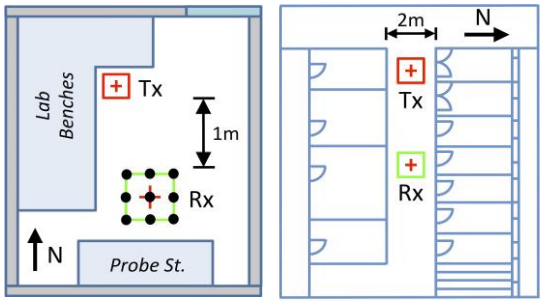

(a) (b)

Fig. 7. Floor plan of (a) shielded room (SR) environment and (b) basement corridor environment (LOS or NLOS, based on orientation of test subject).

The second physical environment was a corridor in the basement of the North-wing of the E-building in Lund University (see Figs. 6(b) and 7(b)). As for SR, the channels were measured for a fixed Tx position and 9 Rx positions (a rectangular grid with 1 λ spacing). For the Rx (terminal prototype with tuners), the same 10 test subjects were measured, but for the FR handgrip only. Depending on the orientations of the test subjects (facing towards or away from the transmit array), the terminal prototype was subjected to either LOS or NLOS conditions relative to the Tx. Since different fading mechanisms could be expected in LOS and NLOS propagation, the two cases are treated separately as LOS and NLOS environments. Overall, the channels were measured for three different propagation environments, 9 Rx positions, 10 test users (of selected grips), and 22 tuner states. The measurement bandwidth was 60 MHz (815-875 MHz, LTE Band 18). However, the data analysis was performed for a 10 MHz bandwidth (840-850 MHz), corresponding to a typical single LTE channel. For the two-hand grips, the same state was used for both tuners, whereas for the one-hand grips, the tuner of the antenna less affected by the hand was set to the 50 Ω state. Even though the reduction in the number of states used saved measurement time, it also reduced the degrees-of-freedom of the AIM to some extent.

All the measured channel data were normalized to their corresponding FS references (i.e., Prototype A with no user in the same environment), in order to analyze the combined (or net) effect of introducing the tuners and user on the terminal performance. In particular, the normalization for the phantom user scenarios (TH-P and OH-P) was performed with respect to the FS reference with only the Prototype A, whereas the normalization for the real user scenarios (FR, FI and OH) was performed relative to the reference case that included a test subject but without the hand(s) in proximity of Prototype A. It should be noted that the use of Prototype A in the reference cases implies that the effects of the tuners remained in the normalized data. A detailed discussion on the normalization procedures for measured MIMO channels is provided in [22].

C. *Figures of Merit*

The system performance of the MIMO prototype with tuners was evaluated in terms of channel capacity, which is a function of correlation, absolute channel gain and channel gain imbalance [23]. To gain insights into the effects of antenna and channel properties on system performance, the capacity-based multiplexing efficiency (ME) metric [24] was used to allow direct comparisons of the contributions from correlation and channel gains in dB. For 2 × 2 MIMO, the capacity with no channel state information (CSI) at the transmitter is [23]

$$C=\log_2\det\left(\mathbf{I}_2+\frac{\rho_{\text{tx}}}{2}\mathbf{H}\mathbf{H}^H\right), \quad (1)$$

where $\mathbf{I}_2$ is the 2 × 2 identity matrix, ρ_{tx} is the SNR at the transmitter, $\mathbf{H}$ is the measured MIMO channel matrix and $(\bullet)^H$ denotes the conjugate transpose operator.

The channel gain per branch measures the average power in the 2 × 2 MIMO channel over N realizations and it is given by

$$G=\sum_{n=1}^{N}\left\|\mathbf{H}^{(n)}\right\|_F^2\Big/4N, \quad (2)$$

where $\|\bullet\|_F$ is the Frobenius norm operator and the index $^{(n)}$ denotes the n-th realization of $\mathbf{H}$. For each free-space reference case (with Prototype A), the channel $\mathbf{H}$ was normalized such that the channel gain was $G=1$ or 0 dB [23]. The same normalization factor was then applied to the channels of cases with user (with Prototype B).

As described in [24], the original ME metric for antenna evaluation [25] was reformulated to include the effect of the propagation channel by replacing the total antenna efficiency with the total channel gain. For the measured channels with the free-space case as the reference, ME was redefined as the equivalent penalty in power (dB) to obtain a given capacity in a given channel, when the tuners and user hand(s) were introduced to the prototype in FS. Any improvement in the absolute ME due to AIM with tuners then measures the power saving due to changes in channel gain and correlation. Therefore, the ME gain from applying the optimal AIM state for capacity (relative to the 50 Ω state) can be written as

$$\Delta\eta_{\text{mux}} = \Delta G + \Delta\eta_{\text{c}}\,(\text{dB}), \tag{3}$$

where $\Delta G = G_{\text{opt}} - G_{50\Omega}\,(\text{dB})$ and $\Delta\eta_{\text{c}} = \eta_{\text{c, opt}} - \eta_{\text{c, 50}\Omega}\,(\text{dB})$ are respectively the change in the channel gain and correlation parts in ME due to AIM. Moreover, $\eta_{c,\,50\Omega} = (1-|r_{50\Omega}|^2)^{1/2}$ and $\eta_{c,\,\text{opt}} = (1-|r_{\text{opt}}|^2)^{1/2}$, where complex correlation coefficients $r_{50\Omega}$ and r_{opt} can be estimated from the receive correlation matrices from the corresponding measured MIMO channels at the 50 Ω ($\mathbf{H}_{50\Omega}$) and optimal ($\mathbf{H}_{\text{opt}}$) states using [24]

$$\mathbf{R}_{\text{rx},50\Omega} = \text{E}\left(\mathbf{H}_{50\Omega}\mathbf{H}_{50\Omega}^{H}\right) = \begin{bmatrix} G_{1,50\Omega} & \sqrt{G_{1,50\Omega}G_{2,50\Omega}}\,r_{50\Omega} \\ \sqrt{G_{1,50\Omega}G_{2,50\Omega}}\,r_{50\Omega}^{*} & G_{2,50\Omega} \end{bmatrix} \tag{4}$$

and

$$\mathbf{R}_{\text{rx,opt}} = \text{E}\left(\mathbf{H}_{\text{opt}}\mathbf{H}_{\text{opt}}^{H}\right) = \begin{bmatrix} G_{1,\text{opt}} & \sqrt{G_{1,\text{opt}}G_{2,\text{opt}}}\,r_{\text{opt}} \\ \sqrt{G_{1,\text{opt}}G_{2,\text{opt}}}\,r_{\text{opt}}^{*} & G_{2,\text{opt}} \end{bmatrix} \tag{5}$$

where $G_{1,50\Omega}$ and $G_{2,50\Omega}$ are the estimated channel gains at antenna ports 1 and 2, respectively, for the 50 Ω state and $G_{50\Omega} = \left(G_{1,50\Omega} + G_{2,50\Omega}\right)/2$. Similarly, $G_{1,\text{opt}}$ and $G_{2,\text{opt}}$ are the channel gains at ports 1 and 2, respectively, for the optimal state and $G_{\text{opt}} = \left(G_{1,\text{opt}} + G_{2,\text{opt}}\right)/2$. $(\bullet)^{*}$ denotes the complex conjugate operator and $\text{E}(\bullet)$ the expectation operator.

Furthermore, to quantify the impact of user on impedance matching, coupling and radiation efficiency, the channels were also measured without the user hand(s) for Prototype B at the 50 Ω state in the SR environment. The change in the channel gains at ports i (ΔG_i) due to the presence of the user hands (still at 50 Ω state) is then due to the combined effect from user-induced changes in matching, coupling and radiation efficiency (with no tuner losses involved). Using the measured S parameters, the matching and coupling efficiencies were $\eta_{1,\text{mc}} = 1-|S_{11}|^2-|S_{21}|^2$ and $\eta_{2,\text{mc}} = 1-|S_{22}|^2-|S_{12}|^2$ for ports 1 and 2, respectively. Therefore, the radiation efficiency could be estimated as $\eta_{i,\text{rad}} = \Delta G_i - \eta_{i,\text{mc}}\,(\text{dB})$ for port i. In this study, the absorption loss by the hand(s) was estimated by the change in the radiation efficiency, since the radiation efficiency change in the lossy metal and dielectrics of the terminal prototype due to the hands was expected to be small.

IV. Results and Analysis

This section focuses on the main results and analysis from the experimental verification. The following steps have been taken in finding the optimal capacity and ME performance: 1) perform a preliminary study on the expected input impedance of the MIMO terminal antennas in various user scenarios; 2) custom-design the impedance tuner coverage region and loss characteristics (adjust inductors L1 and L2 on Fig. 1) to best suit the coverage required for the expected input impedances; 3) choose tuner states (with denser states around the expected impedances) for experimental verification and implement the custom-designed AIM system on the handset; 4) perform real-world propagation measurements in all chosen states and user scenarios and post-process results to evaluated ME and MIMO capacity in all cases; 5) find optimal states based on the system level metrics and evaluate net gain (losses considered). Analysis of the channel measurements also confirmed that having denser states around the conjugate of measured input impedance for relevant user scenarios successfully captured the optimal states for capacity and ME.

A. AIM Potential in Two-Hand Real User Scenarios

This section analyzes the potential of AIM to compensate for user-induced degradation in two-hand real user scenarios.

1) Channel Gain

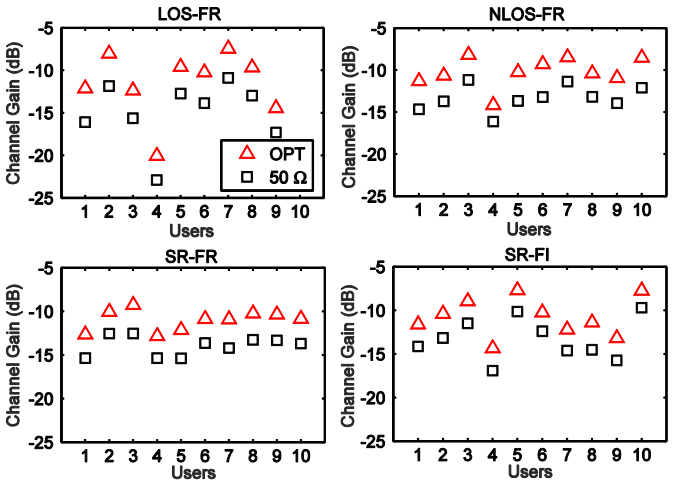

Fig. 8. MIMO channel gain of 10 users in 4 channel-user configurations with 50 Ω and optimal (OPT) states.

Figure 8 presents the normalized channel gain per branch in all environments for all users, both before (50 Ω state) and after AIM (optimal state), except for User 10 in the LOS-FR scenario, due to corrupted measurement data. The channel gain was averaged over 10 MHz (840-850 MHz) and it reflects both user-induced degradation and tuner losses. Given the tuner losses of 1 dB at the 50 Ω state, user interaction alone resulted in severe degradations in channel gains of at least 8.7 dB over all cases. Measurements of the hand size of the users indicate significant differences in length (168 mm to 210 mm), width (73 mm to 127 mm) and volume (220 ml to 500 ml). Further analysis reveals that there is a clear trend between the hand volume and the channel gain, i.e., the larger the hand volume, the smaller the channel gain (i.e., the larger the user-induced loss). For example, the user with the largest hand volume (user 4) has the lowest channel gain. A similar trend was observed between the hand width and the channel gain (i.e., a larger width gives a lower channel gain).

Nevertheless, the trend is less obvious between the hand length and channel gain. This can be explained by the physical coverage of antenna elements at the shorter edges by the two-hand grip being influenced mostly by the hand width and volume, rather than the hand length that mainly determines the extension of the bent fingers. These results confirm that the hand size has a significant influence on user-induced losses and therefore the expected channel gain.

Nevertheless, the AIM system that optimized the capacity was effective in mitigating the degradation in all cases, with the largest gain improvement of 4 dB achieved for User 1 in the LOS-FR case (see Fig. 8). It is noted that the gain improvements account for the increased tuner losses at the optimal states of the respective cases relative to the 50 Ω state.

2) Capacity

To consider the benefit of AIM on the link or system level, the average capacity with no CSI is presented in Table II, for the reference SNR of 20 dB. Here, the capacity was averaged over the evaluation bandwidth of 10 MHz as well as over the users tested in each channel-user case. The achieved capacity gains when averaged over users range from 31% in the SR-FI scenario to 42% in the LOS-FR scenario. These results are consistent with those from earlier studies using ideal tuners simulated in post-processing [7], [8], where capacity gains from 43% to 50% were found for a two-hand grip in both simulated and measured environments.

In Fig. 9, the variations in capacity over the 22 measured states are illustrated for a free-space measurement and a representative channel-user case (User 3 in the SR-FI case). As can be observed in Fig. 9(a), the optimal state for the FS case is close to 50 Ω. This is because the terminal prototype was well-matched in free-space. On the other hand, the firm (FI) grip severely mismatched the antenna, such that the optimal state in Fig. 9(b) was at VSWR = 2.6. Using identical states on both tuners, an overall capacity gain of 1.3 bits/s/Hz (4.7 to 6.0 bits/s/Hz) was obtained for this case.

TABLE II
AVERAGE MIMO CAPACITY AT 50 Ω VS. OPT STATE AND % CAPACITY GAIN

Capacity (bits/s/Hz)	LOS-FR	NLOS-FR	SR-FR	SR-FI
@ 50 Ω	3.1	3.7	3.7	3.8
@ OPT	4.4	5.0	5.0	5.0
Gain (%)	42	36	35	31

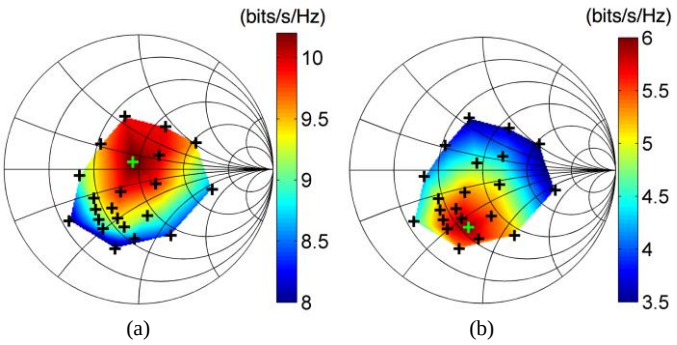

Fig. 9. Average MIMO capacity: (a) FS in SR and (b) User 3 in SR-FI; black (+) – states measured; green (+) – optimal state

It was described in Section II that tuner losses strongly affect the location of optimal tuner states as well as the achievable AIM gains. In order to better explore the effect of tuner losses, the optimal state for User 3 in the SR-FI setup was calculated for the lossless case by de-embedding the tuner losses from the measurement. It was found that in the lossless case, the optimal state for capacity was further away from the center of the Smith chart, towards the conjugate of the antenna input impedance at VSWR = 4.2. This is because in general, the tuner losses increase with VSWR (see Fig. 2(b)), hence requiring a tradeoff between minimizing both mismatch and tuner loss to achieve the optimal capacity.

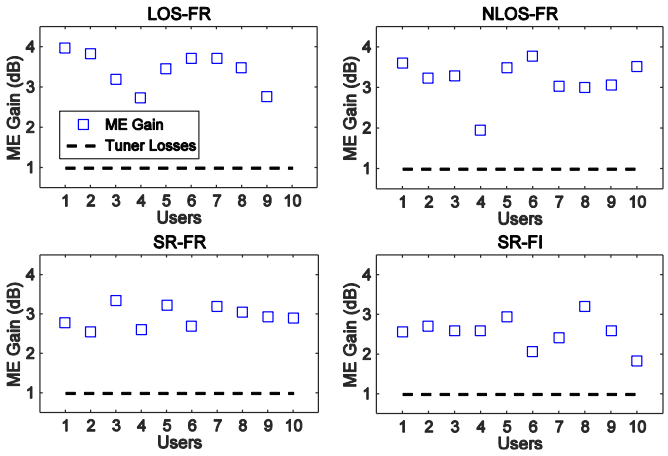

Fig. 10. ME gain of 10 users in four channel-user setups.

3) Multiplexing Efficiency

Expressing AIM gain in terms of ME allows tuner losses to be subtracted directly (in dB) to obtain the net equivalent power gain from AIM. In particular, the ME gains (optimal tuner state vs. 50 Ω state) of all channel-user cases were calculated from the normalized measured channels and plotted in Fig. 10. Since these ME gains were obtained relative to the 50 Ω state, the difference in tuner losses between the optimal and the 50 Ω states were implicitly accounted for. Therefore, the net ME gain can be estimated by subtracting the 1 dB tuner losses at the 50 Ω state. As can be seen in Fig. 10, the ME gains range from 1.8 to 4 dB, which implies net ME gains from 0.8 to 3 dB, confirming that significant net performance gains were achieved, even for the realistic tuners considered in this study.

The results in Fig. 10 suggest that the variations in ME gains among users in any given channel are fairly small (mostly within about 1 dB), except for User 4 in the NLOS-FR case. To explain the outlier, a comparative analysis was performed for User 4 and a representative user (User 5) in NLOS-FR. The results are given in Table III in terms of user-induced changes (relative to FS) in radiation efficiency $\Delta\eta_{\mathrm{rad}}$ (i.e., absorption loss) and matching/coupling efficiency $\Delta\eta_{\mathrm{mc}}$, averaged over the two antenna ports and a 10 MHz bandwidth. To obtain the actual values of $\Delta\eta_{\mathrm{rad}}$ and $\Delta\eta_{\mathrm{mc}}$ at the antenna ports, the tuner loss was de-embedded from the measured results. It can be seen in Table III that $\Delta\eta_{\mathrm{mc}}$ is similar between the two users (-6.3 vs. -6.4 dB), where User 4 has nearly 3 dB higher absorption loss ($-\Delta\eta_{\mathrm{rad}}$) than User 5. The

difference in absorption loss can be attributed to the palm and finger sizes of Users 4 and 5, with User 4 having significantly larger palms and thicker fingers. Nevertheless, these behaviors in $\Delta\eta_{mc}$ and $\Delta\eta_{rad}$ do not account for the significantly smaller ME gain in User 4. Table III also shows the contributions of channel gain and correlation to the ME gain (i.e. ΔG and $\Delta\eta_c$), indicating that the AIM provided the ME gains mainly by improving the channel gains. However, despite the similarity in $\Delta\eta_{mc}$, ΔG for User 4 was 1.4 dB lower than that for User 5. Further investigation revealed that despite having similar $\Delta\eta_{mc}$, the optimal states for capacity were different for the two users, i.e., State #257 for User 4 and State #261 for User 5 in Fig. 2(b). As can be seen in Fig. 2(b), both states are in the "yellow region" with similar tuner losses, but with different VSWRs (higher VSWR for User 5 than User 4). This means that when optimizing for capacity, AIM had greater flexibility to reduce impedance mismatch for User 5 than for User 4 without increasing tuner losses.

TABLE III
CHANGE IN RADIATION EFFICIENCY, MISMATCH/COUPLING EFFICIENCY (USER VS. FS), CHANNEL GAIN, CORRELATION GAIN (OPTIMAL VS. 50 Ω) FOR USERS 4 AND 5 IN NLOS-FR AND USER 10 IN SR-FI

	NLOS-FR		**SR-FI**
	User 4	**User 5**	**User 10**
$\Delta\eta_{mc}$ (dB)	-6.3	-6.4	-2.8
$\Delta\eta_{rad}$ (dB)	-8.9	-5.8	-5.7
ΔG (dB)	2.0	3.4	2.0
$\Delta\eta_c$ (dB)	-0.02	0.06	-0.l5

TABLE IV
CHANNEL GAINS, CORRELATION GAIN AND MULTIPLEXING EFFICIENCY GAIN

	FR	**FI**	**TH-P**	**OH-P**	**OH**
$G_{50\Omega}$ (dB)	-13.8	-12.7	-7.7	-0.9	-6.4
G_{opt}(dB)	-10.9	-10.3	-5.7	-0.6	-6.1
ΔG (dB)	2.9	2.4	1.9	0.3	0.4
$\Delta\eta_c$ (dB)	0.01	0.02	0.07	0.08	-0.01
$\Delta\eta_{mux}$ (dB)	2.9	2.4	2.0	0.4	0.4

B. User Hand Grip Effects on AIM Performance

To investigate the effect of user model (real user vs. phantom) as well as handgrip (FR, FI, OH-P, TH-P and OH) on AIM performance, Table IV presents the channel gains at the 50 Ω and optimal states, the channel gain difference ΔG and the correlation gain $\Delta\eta_c$ for the five handgrips tested in this study, averaged over the users in each case. All five grips were measured in the SR environment.

Apart from non-uniform tuner loss distribution with VSWR, low ME gains were also observed to be the result of low impedance mismatch. This can be illustrated using User 10 in the SR-FI setup. As can be seen in Table III, in this case, the matching/coupling efficiency was degraded by only 2.8 dB when the hands were introduced. Therefore, the ME gain was low (1.8 dB) even though AIM could compensate for most the efficiency loss (i.e., $\Delta G = 2$ dB). Again, due to the low correlation of Prototype B, the impact of correlation on the ME gain was negligible. To examine the possible impact of the limited number of chosen states on the ME gains across users, it was confirmed that the optimal state for capacity in all the channel-user setups was captured inside the boundary of the 22 states. Moreover, the ME variation between the optimal state and the second best state for capacity was small (typically around 0.2 dB), indicating that the finite number of states has little impact on the differences in the results.

It was shown in [7], [9] and [26] that hand/finger location with respect to the antenna critically affects impedance matching, and hence potential benefits from AIM. In this work, we confirmed these findings with both phantoms (OH-P and TH-P) and real users (FR, FI and OH). From the results in Table IV, it can be seen that the one-hand grips do not degrade antenna performance as severely as the two-hand grips. This is because only one antenna is covered by the one-hand grips, as compared to both antennas being covered in the two-hand grips (e.g., $G_{50\Omega}$ = -6.4 dB for OH vs. -12.7 dB for FR). This also resulted in lower ME gain from AIM (up to 0.4 dB for one-hand grips vs. up to 2.9 dB for two-hand grips).

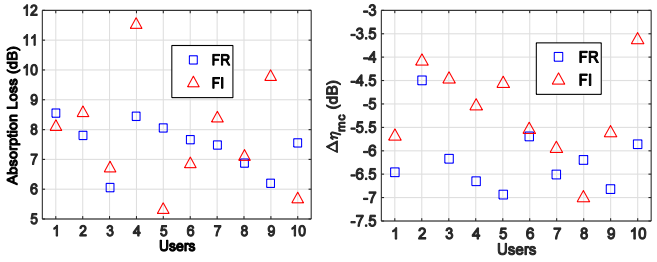

Fig. 11. User-induced absorption loss ($-\Delta\eta_{rad}$) and change in matching and coupling efficiency ($\Delta\eta_{mc}$) for FR and FI in SR.

Figure 11 shows the absorption loss ($-\Delta\eta_{rad}$) and change in matching/coupling efficiency ($\Delta\eta_{mc}$) for all 10 users in the FR and FI grips, relative to free-space (no AIM) and averaged over both ports. Overall, 9 out of 10 user cases have lower $\Delta\eta_{mc}$ in the FR case as compared to FI, indicating higher losses in the FR handgrip. When averaged over all 10 users, $\Delta\eta_{mc}$ is 5.3 dB and 4.3 dB for FR and FI, respectively. This result is counterintuitive, since the FI grip as shown in Fig. 5(a) offered a full coverage of the shorter edges of the terminal (i.e., the antenna locations), which should mismatch the antennas more severely. However, a closer examination revealed that in the FR grip shown in Fig. 5(b), the fingers formed a tighter grip around the antenna elements responsible for the low band resonance which led to a 1 dB higher matching/coupling loss on average. This contributed to the 0.5 dB difference in ΔG between the FR (2.9 dB) and FI grip (2.4 dB) grips in Table IV. Given low coupling in Prototype B, this result (based on real users and real tuners) confirms the earlier observation in [7] that AIM can in general offer higher performance improvements in cases of higher mismatch.

In Fig. 11, significant variations in absorption loss can be observed across the 10 users for both grip styles. In the FR case, the variations are up to 2.6 dB (8.6 dB for User 1 vs. 6 dB for User 3), whereas in the FI grip, larger variations of up to 6.2 dB are measured (11.5 dB for User 4 vs. 5.3 dB for User 5). This is due to the setup of both grip styles. The FI grip is more individual, as it depends heavily on the size of the hands that covers the terminal antennas, with larger hands causing

higher absorption losses. However, in the FR grip, the users were observed to cover a smaller part of the terminal antennas, resulting in a smaller dependence of absorption loss on the hand size. However, the closer proximity of the hand to the antennas in FR than FI resulted in comparable average absorption loss over all users. These results confirm the earlier work in [27], where large variations in absorption loss of up to 9 dB among users were found.

Furthermore, it was found in [15] that real users could lead to significantly different mismatch losses as compared to phantoms. This observation is consistent to the results in this study, where the average mismatch losses for FR and FI were 5.3 dB and 4.3 dB, respectively, whereas for TH-P the loss was 2.6 dB. Since the extent of mismatch largely determines the AIM gain potential, the mismatch loss difference between real users and phantoms results in lower AIM gains for the phantom cases (1.9 dB vs. 2.4 dB for TH-P vs. FI). This suggests that existing phantoms tend to underestimate the true potential of AIM. The primary reason for the lower impact of the phantom hands is the lack of flexibility (in gripping the prototype) and the limited availability of phantom hand size for different terminal form factors, leading to less realistic and more relaxed grip styles. Moreover, the phantom hands were homogenous in composition, whereas the human hands were heterogeneous and vary among test subjects [26].

C. Propagation Effects on AIM Performance

Apart from being distinct realistic operating scenarios, the three propagation environments (SR, LOS and NLOS) were also chosen to provide channels with different propagation characteristics with respect to angular spread. In particular, SR is a rich multipath environment (i.e., uniform 3D angular distribution), LOS being an environment with limited angular spread, and NLOS having an angular spread in between SR and LOS. To verify that this aim is achieved, Fig. 12 shows the eigenvalue spreads of the three channels in terms of ellipticity statistic (ES) [28]. A higher angular spread leads to a lower eigenvalue spread and a higher ES value. The SR case is confirmed to be close to the ideal rich multipath case of independent and identically distributed (IID) Rayleigh channels, whereas ES is lowest for LOS.

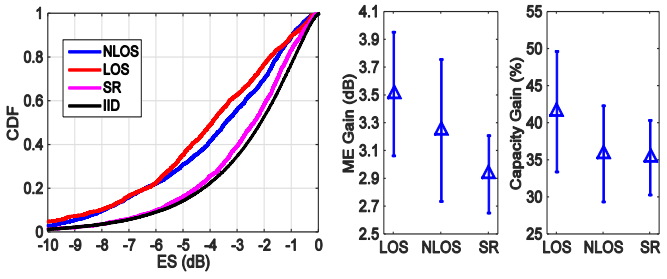

Fig. 12. Ellipticity statistic (ES) as well as mean and standard deviation of ME gain and capacity for FR in three measured environments.

To analyze the effects of different angular spreads in SR, LOS and NLOS on AIM performance, Fig. 12 also presents the average and standard deviation of the ME and capacity gains over 10 users in these environments. The average ME gains are 3.5 dB, to 3.2 dB and 2.9 dB in LOS-FR, NLOS-FR and SR-FR, respectively, indicating only minor gain variations (up to 0.6 dB) that are within experimental errors, including the use of finite tuner states and the limited ability of each user to reproduce the exact same FR grip in all three environments. Similarly, the small average capacity gain variation between 35% (SR-FR) and 42% (LOS-FR) confirms at best weak dependence of the capacity gain on the propagation channel. Furthermore, it was found that the ME gains were primarily attributed to change in the channel gain ΔG, with the change in correlation gain $\Delta\eta_c$ being less than 0.1 dB in all cases.

Nevertheless, this finding does not contradict with earlier observations that different propagation environments can lead to different capacity gains from AIM [7], [9]. This is because in the SR environment, Prototype B (0.2) offered significantly lower envelope correlation than Prototype A (0.5), based on which the conclusions in [7] and [9] were drawn. In particular, two primary mechanisms were found to explain the different capacity gains. Firstly, for a propagation channel with a narrow angular spread at the receiver, only a limited angular region of the receive antenna patterns will be illuminated. Therefore, the amount of received power depends on the local behavior of the antenna patterns. In cases where AIM offers improved efficiency from mismatch compensation (i.e., no change in the shapes of the antenna patterns, as in Prototype B), only a power gain (i.e., ΔG) is achieved with AIM. However, this power gain occurs at different received powers (SNRs) when different regions of the patterns are illuminated. In this scenario, capacity gain can differ due to capacity being a logarithmic function of SNR [7], [9]. However, the measured channels in this study were normalized to the FS references, which lead to similar average channel gains (see Fig. 8) and hence similar effective SNRs for capacity evaluation under different environments. This accounts for the minor variations seen in the capacity and ME gains.

On the other hand, optimizing AIM for capacity can also lead to different antenna pattern shapes and hence correlations, relative to the 50 Ω state [9]. In this case, the achieved capacity gain with AIM is the result of changes in both the received power and correlation. However, for the simple uncoupled matching networks [3], [4] used in this study, changes in correlation can only occur when the MIMO antennas show high coupling and pattern correlations. Since Prototype B offers low correlations, this mechanism does not apply here.

V. Conclusions

In this work, a practical AIM system with two custom-designed CMOS-SOI impedance tuners was implemented on a MIMO terminal prototype with a standalone battery unit and experimentally verified by a first of its kind AIM system measurement in realistic propagation conditions. The applicability of AIM to improve MIMO performance in severe user interaction scenarios was probed in a shielded room (SR) and an office corridor (LOS and NLOS), involving 10 test subjects. The measured results revealed ME gains of up to 4 dB over all channel-user setups. Moreover, the average ME gain for the LOS environment was 3.5 dB (or 2.5 dB including tuner losses), which established the promising potential of AIM to improve system performance in realistic propagation conditions. The large ME gain was mainly obtained from improved channel gains, as the low pattern correlation in the

prototype with the tuners largely limited the ability of the uncoupled tuner system to adapt the antenna patterns for a trade-off between correlation and received power for optimal capacity. This also resulted in only minor variations in the capacity and ME gains for environments with different AS.

Notwithstanding, it was found that apart from the extent of user-induced impedance mismatch, the distribution of the tuner losses also contributed to the difference in ME gains for different users. Furthermore, the optimal state for capacity in each case involved a tradeoff between mismatch compensation and tuner losses. In addition, phantom handgrips were compared to real user handgrips. It was established that due to their size, flexibility and composition, phantom hands led to significantly lower impedance mismatch than real hands. Therefore, the phantom hands provided only a conservative estimate of the performance gain with AIM.

It is noted that the channel measurement system with Prototype B has been developed as a technology demonstrator, allowing real-time user effect compensation by the tuners to be observed using LabView and a VNA. Possible future work includes further reduction in the losses of the CMOS-SOI tuners by using lower-loss PCBs and flip-chip mounting to mitigate parasitic inductances. Moreover, instead of an exhaustive sweep of selected tuner states, an AIM algorithm can be developed for the convergence to the optimal state. Finally, the use of coupled matching networks [29] would facilitate even higher AIM gains, due to a greater flexibility to modify the antenna patterns for optimum capacity.

ACKNOWLEDGMENT

We thank Zachary Miers of Lund University for his support with the digital control of the impedance tuners. We are grateful to all the test subjects who participated in the measurement campaign. We also thank STMicroelectronics for sponsoring the tuner chip fabrication.

REFERENCES

[1] "CTIA test plan for wireless device over-the-air performance," Revision 3.2.3, CTIA Wireless Association, Jul. 2014.

[2] B. K. Lau, "Multiple antenna terminals," in *MIMO: From Theory to Implementation*, C. Oestges, A. Sibille, and A. Zanella, Eds. San Diego: Academic Press, 2011, pp. 267-298.

[3] J. B. Andersen and B. K. Lau, "On closely coupled dipoles in a random field," *IEEE Antennas Wireless Propag. Lett*., vol. 5, pp. 73-75, 2006.

[4] B. K. Lau and J. B. Andersen, "On closely coupled dipoles with load matching in a random field," in *Proc. IEEE Int. Symp. Personal, Indoor, Mobile Radio Commun. (PIMRC'2006)*, Helsinki, Finland, Sep. 11-14, 2006.

[5] Y. Fei et. al., "Optimal single-port matching impedance for capacity maximization in compact MIMO arrays," *IEEE Trans. Antennas Propag*., vol. 56, no. 11, pp. 3566-3575, Nov. 2008.

[6] I. Vasilev, E. Foroozanfard, and B. K. Lau, "Adaptive impedance matching performance of MIMO terminals with different bandwidth and isolation properties in realistic user scenarios," in *Proc. 7th Europ. Conf. Antennas Propag. (EuCAP'2013)*, Gothenburg, Sweden, Apr. 8-12, 2013, pp. 2590-2594.

[7] I. Vasilev, V. Plicanic, and B. K. Lau, "Impact of antenna design on MIMO performance for compact terminals with adaptive impedance matching," *IEEE Trans. Antennas Propag*., in revision. [original manuscript attached to this submission]

[8] V. Plicanic, I. Vasilev, R. Tian, and B. K. Lau, "Capacity maximisation of handheld MIMO terminal with adaptive matching in indoor environment," *IET Electron. Lett.*, vol. 47, no. 16, pp. 900-901, 2011.

[9] I. Vasilev, V. Plicanic, R. Tian, and B. K. Lau, "Measured adaptive matching performance of a MIMO terminal with user effects," *IEEE Antennas Wireless Propag. Lett*., vol. 12, pp. 1720-1723, 2013.

[10] P. Sjöblom and H. Sjöland, "An adaptive impedance tuning CMOS circuit for ISM 2.4-GHz band," *IEEE Trans. Circuits Syst. I*, vol. 52, no. 6, pp. 1115-1124, Jun. 2005.

[11] A. S. Morris III, Q. Gu, M. Ozkar, and S. P. Natarajan, "High performance tuners for handsets," in *Proc. IEEE Microw. Theory Techn. Symp. (MTT'2011)*, Baltimore, MD, Jun. 5-10, 2011.

[12] F. Sonnerat et. al., "30 dBm P_{1dB} and 4dB insertion losses optimized 4G antenna tuner fully integrated in a 130nm CMOS SOI technology," in *Proc. Radio Wireless Symp. (RWS'2013)*, Austin, TX, Jan. 20-23, 2013.

[13] S. Hu, et al., "Atenna impedance variation compensation by exploiting a digital doherty power amplifier architecture," *IEEE Trans. Microw. Theory Techn*., vol. 63, no. 2, pp. 580-597, Feb. 2015.

[14] S. M. Ali, et al., "Dynamic measurement of complex impedance in real-time for smart handset applications," *IEEE Trans. Microw. Theory Techn*., vol. 61, no. 9, pp. 3453-3460, Sep. 2013.

[15] K. R. Boyle, et al., "Gain statistics for mobile phone antenna tuners," in *Proc. Europ. Conf. Antennas Propag. (EuCAP'2013)*, Gothenburg, Sweden, Apr. 8-12, 2013, pp. 424-428.

[16] J. Lindstrand, I. Vasilev, and H. Sjöland, "A low band cellular terminal antenna impedance tuner in 130nm CMOS-SOI technology," in *Proc. Europ. Solid State Circ. Conf. (ESSCIRC'2014)*, Venice, Italy, Sep. 22-26, 2014, pp. 459-462.

[17] G. M. Rebeiz and J. B. Muldavin, "RF MEMS switches and switch circuits," *IEEE Microw. Mag.*, vol. 2, no. 4, 2001.

[18] [Online]. Available: http://www.atmel.com/devices/ATMEGA32.aspx

[19] K. Boyle and M. Leitner, "Mobile phone antenna impedance variations with real users and phantoms," in *Proc. Int. Workshop Antenna Technol. (IWAT'2011)*, Hong Kong, China, Mar. 7-9, 2011.

[20] H. Li, Z. Miers, and B. K. Lau, "Design of orthogonal MIMO handset antennas based on characteristic mode manipulation at frequency bands below 1 GHz," *IEEE Trans. Antennas Propag*., vol. 62, no. 5, pp. 2756-2766, May 2014.

[21] Z. Miers, H. Li, and B. K. Lau, "Design of bandwidth enhanced and multiband MIMO antennas using characteristic modes," *IEEE Antennas Wireless Propag. Lett*., vol. 12, pp. 1696-1699, 2013.

[22] R. Tian, V. Plicanic, B. K. Lau, and Z. Ying, "A compact six-port dielectric resonator antenna array: MIMO channel measurements and performance analysis," *IEEE Trans. Antennas Propag*., vol. 58, no. 4, pp. 1369-1379, Apr. 2010.

[23] A. Paulraj, R. Nabar, and D. Gore, *Introduction to Space-Time Wireless Communications*. New York: Cambridge University Press, 2003.

[24] R. Tian et. al., "Multiplexing efficiency of MIMO antennas in arbitrary propagation scenarios," in *Proc. Europ. Conf. Antennas Propag. (EuCAP'2012)*, Prague, Czech Republic, Mar. 26-30, 2012, pp. 373-377.

[25] R. Tian et. al., "Multiplexing efficiency of MIMO antennas," *IEEE Antennas Wireless Propag. Lett*., vol. 10, pp. 183-186, 2011.

[26] M. Pelosi et al.,"A grip study for talk and data modes in mobile phones," *IEEE Trans. Antennas Propag.*, vol. 57, no. 4, pp. 856-865, Apr. 2009.

[27] G. F. Pedersen, K. Olesen, and S. L. Larsen, "Bodyloss for handheld phones," in *Proc. Vehicular Techn, Conf. (IEEE VTC 1999)*,Houstan, TX, USA, Jul. 1999, vol. 2, pp. 1580-1584.

[28] J. Salo, P. Suvikunnas, H. M. El-Sallabi, and P. Vainikainen, "Ellipticity statistic as a measure of MIMO multipath richness," *Electron. Lett.*, vol. 42, no. 3, pp. 45-46, Feb. 2006.

[29] J. Weber, et al. "Miniaturized antenna arrays using decoupling networks with realistic elements," *IEEE Trans. Microw. Theory Techn*., vol. 54, no. 6, pp. 2733 -2740, Jun. 2006.